SCIENCE CHINA
Information Sciences

• RESEARCH PAPER •

May 2023, Vol. 66 152304:1–152304:9
https://doi.org/10.1007/s11432-022-3564-2

Low-loss wide-bandwidth planar transmission line with a laminated conductor

Ken NING, Xiao-Chun LI*, Yan SHAO* & Junfa MAO

Key Laboratory of Ministry of Education of Design and Electromagnetic Compatibility of High-Speed Electronic Systems, Shanghai Jiao Tong University, Shanghai 200240, *China*

Received 8 April 2022/Revised 13 June 2022/Accepted 27 July 2022/Published online 20 April 2023

Abstract In this paper, the laminated conductor technology is first introduced to planar-integrated transmission lines. The laminated conductor is composed of multilayers of metal and insulator, which has a lower conductor loss than a solid conductor. Based on the silicon-based micro electromechanical system technology, a laminated coplanar waveguide (CPW) with wide bandwidth and low loss is proposed, which uses a laminated conductor for signal lines and grounds. A laminated CPW and its transition are designed, fabricated, and measured. The simulation results show that the laminated CPW with many insulator layers has a low conductor loss. The measurement results illustrate that the average insertion loss of the laminated CPW is 0.65 dB from DC to 40 GHz, which is 44.4% smaller than that of the solid CPW.

Keywords coplanar waveguide (CPW), laminated conductor, conductor loss, skin effect, silicon-based technology, wide-bandwidth

Citation Ning K, Li X-C, Shao Y, et al. Low-loss wide-bandwidth planar transmission line with a laminated conductor. Sci China Inf Sci, 2023, 66(5): 152304, https://doi.org/10.1007/s11432-022-3564-2

1 Introduction

The development of miniaturized, high-performance, and low power consumption integrated circuits has never stopped [1, 2]. With the operating frequency dramatically increasing and the feature size quickly decreasing, the power consumption of interconnects, which is mainly caused by conductor and dielectric losses, has become increasingly considerable. Such losses increase with frequency. In particular, the conductor loss rapidly deteriorates due to the skin effect [3], which becomes highly prominent as the feature size decreases.

To improve the performance of interconnects, many approaches have been introduced [4–19]. Superconductor interconnects [4–9] were proposed for their nearly loss-free property. Graphene [10, 11] and nanofiber [12, 13] interconnects were presented for their excellent thermal and electrical conductivities. However, these interconnects were limited by temperature conditions or the high process complexity and cost. In [14, 15], the conductor loss of a printed transmission line was improved using two symmetrical metal layers, where a suspended stripline [15] with symmetrical metal worked from 8 to 11 GHz, and its conductor loss was reduced by 30% at 10 GHz. Introducing negative-permeability material layers alternately stacked with Cu layers increased the skin depth and reduced the conductor loss [16–19], where negative-permeability materials were ferromagnetic materials, such as NiFe [16, 17], CoZrNb [18], and Co [19]. For instance, a coplanar waveguide (CPW) using stacked Cu and Co layers [19] operated from DC to 32 GHz, with the loss reduced up to 50% at 28 GHz. However, the structure of ferromagnetic materials may suffer from electromagnetic compatibility (EMC) problems.

Laminated conductors were used for coaxial cable design [20–22], which increased the effective skin depth and reduced the conductor loss. In this cable, the inner conductor is composed of a non-conducting core surrounded by alternating layers of conductors and insulators, and the outer conductor is the solid conductor. Compared with the conventional coaxial cable using solid metal as its inner and outer conductor, the laminated coaxial cable can reduce the conductor loss by 40% at 12 MHz.

* Corresponding author (email: lixc@sjtu.edu.cn, shaoyan2009@sjtu.edu.cn)

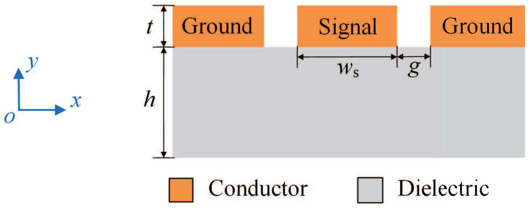

Figure 1 (Color online) Structure of the solid CPW.

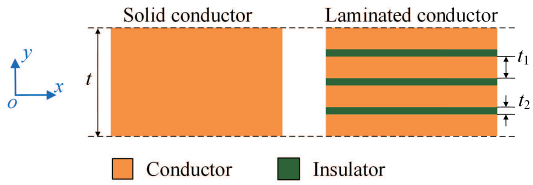

Figure 2 (Color online) Structures of the solid conductor and laminated conductor.

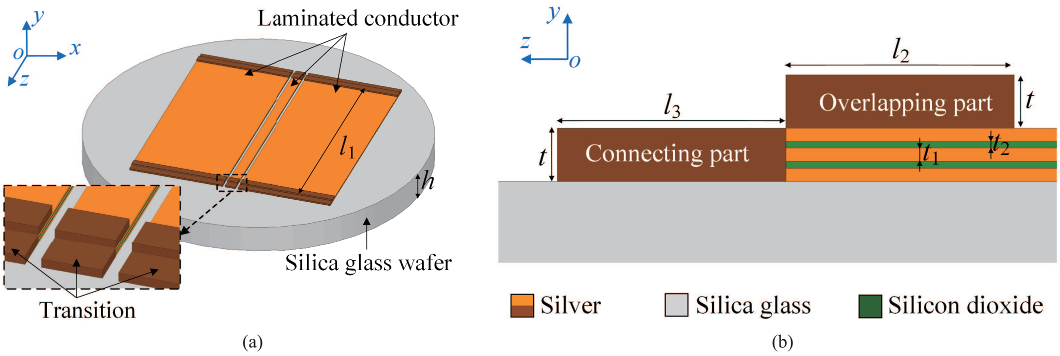

Figure 3 (Color online) Structure of the silicon-based laminated CPW with transitions. (a) Structure of the laminated CPW with the transitions in the 3D view; (b) structure details of the transition in the *yoz* section view.

In this paper, the laminated conductor technology is first introduced to planar-integrated transmission lines. Based on the silicon-based microelectromechanical system (MEMS) technology, a low-loss laminated CPW with wide bandwidth is proposed, where the signal line and grounds are both equipped with laminated conductors. The loss of the laminated CPW is much smaller than that of the solid CPW since the effective skin depth of the laminated CPW is larger than that of the solid CPW, and the laminated CPW with many insulator layers shows a low conductor loss. Furthermore, replacing the solid conductor with the laminated conductor has nearly no impact on the characteristic impedance, phase constant, and dielectric attenuation of the CPW. A laminated CPW with two layers of insulators and a solid CPW are designed, fabricated, and measured. From DC to 40 GHz, the average insertion loss of the laminated CPW is 44.4% smaller than that of the solid CPW.

This paper is organized as follows. In Section 2, the structure of the laminated CPW and its fabrication process are introduced. In Section 3, the propagation properties of the laminated CPW are analyzed. In Section 4, a detailed experimental verification is given. Finally, in Section 5, a brief conclusion is summarized.

2 Laminated planar transmission line

Figure 1 shows the structure of a conventional CPW with a solid conductor. A center signal line and two side grounds are in the same conductor layer, where the conductor thickness is t. The substrate thickness, signal width, and gap width are denoted as h, w_{s}, and g, respectively.

To reduce the conductor loss of the CPW, the laminated conductor was used to replace the solid conductor. As shown in Figure 2, the laminated conductor was formed of alternately stacked conductor and insulator layers, where the thicknesses of the conductor and insulator layers are t_1 and t_2, respectively. Moreover, the total thickness of the laminated conductor is equal to the thickness of the solid conductor. The number of layers of the laminated conductor is arbitrary, and only the number of insulator layers is required to be greater than or equal to 1.

2.1 Silicon-based laminated CPW

Figure 3(a) shows the laminated CPW with its transition structure based on silicon-based MEMS technology. The laminated conductor is composed of stacked silver layers and silicon dioxide (dielectric constant

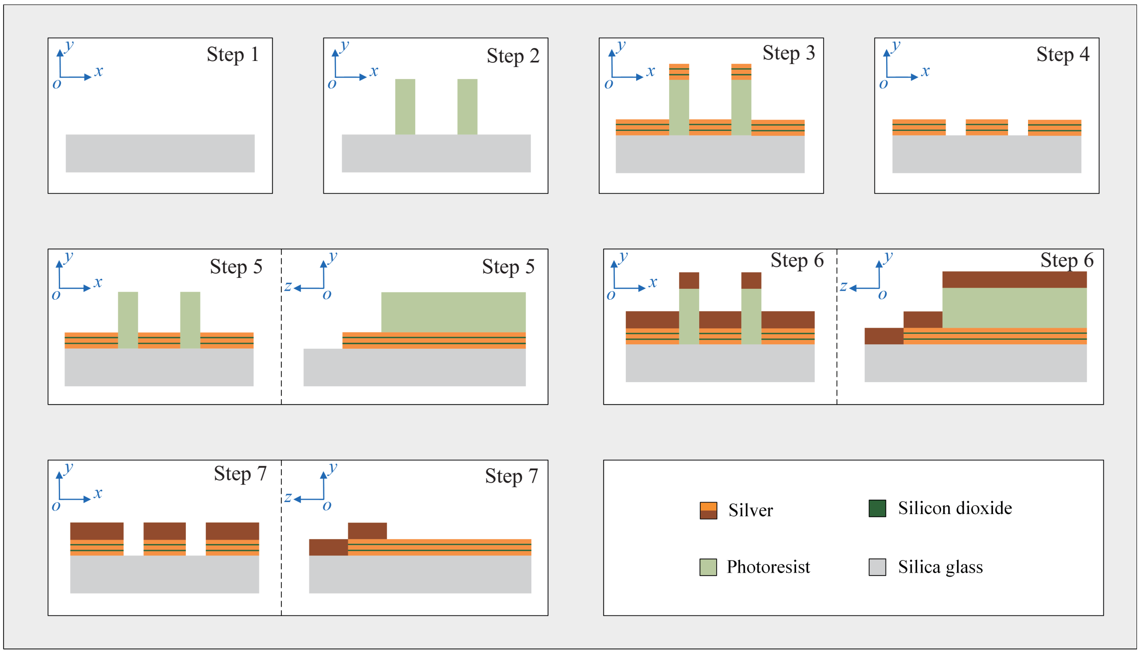

Figure 4 (Color online) Fabrication steps of the laminated CPW with the transitions.

$\epsilon_1 = 4$) layers. Silica glass wafer (dielectric constant $\epsilon_2 = 4.7$, loss tangent $\tan\delta = 0.0005$) is used as the substrate with a thickness h of 1 mm. The length of the laminated CPW is l_1. To ensure reliable contact among the metal layers of the laminated conductor, silver blocks are designed at the terminals of the laminated CPW as the transitions, as shown in Figure 3(b). The transitions are fabricated through one-time lithography and metal deposition, which are deliberately designed to overlap the laminated body for a stable connection between the transitions and the laminated body. Thus, the transition is divided into the connecting part with the length l_2 and the overlapping part with the length l_3, which are staggered in height. As the length of the overlapping part is designed much shorter than that of the laminated CPW, the impact of the overlapping part on the performance can be ignored. The thickness of the two parts is equal to that of the laminated conductor t.

2.2 Fabrication processes

The fabrication of the proposed laminated CPW with transition is performed in a super-clean laboratory with two-time lithography to make the laminated conductor and transition. In Figure 4, the fabrication steps are introduced. Wafer cleaning and the first lithography in the view of the xoy section are from step 1 to step 4, and the second lithography in the views of the xoy and yoz sections are from step 5 to step 7. The detailed process steps are given as follows.

Step 1. The substrate is cleaned. First, the silica glass wafer is immersed in acetone for ultrasonic cleanout. Second, the wafer is ultrasonically cleaned using anhydrous alcohol. Third, the wafer is ultrasonically cleaned with isopropanol to prevent the wafer from being soiled by airborne particles. In each supersonic cleanout, the temperature is 50°C and the washing time is 5 min. Finally, the wafer is spun, rinsed, and dried.

Step 2. The first lithography is performed to make all the laminated layers with the same graphic. Specifically, the photoresist AZ 6030 is spun-coated on the substrate, and then the exposure of the photoresist is made under the mask of the laminated structure. Finally, the photoresist development is made, and the graphic is obtained.

Step 3. The laminated layers are deposited, in which silver layers are deposited via evaporation, and silicon dioxide layers are prepared via plasma-enhanced chemical vapor deposition. For the proposed line with an arbitrary number of laminated layers, the fabrication process is similar, except for the number of deposition times.

Step 4. The lift-off process is performed to remove the photoresist and obtain the laminated conductor body.

Step 5. The second photoresist process is carried out to make the transition structures. The detailed process is similar to step 2.

Step 6. The transition structure layer is deposited via evaporation.

Step 7. The lift-off process is performed to remove the photoresist, and the transition structure graphic is obtained.

Until now, the fabrication process of the proposed laminated CPW with transition has been completed.

3 Propagation properties of the laminated CPW

3.1 Principle

High-frequency electromagnetic waves can penetrate only a limited distance into the interior of a good conductor. This phenomenon is known as the skin effect. The current density decreases to e^{-1} when the distance into the interior of the conductor increases to $\delta_{\rm s}$, which can be calculated as [23]

$$\delta_{\rm s} = \sqrt{\frac{2}{\omega\mu\sigma}}, \tag{1}$$

where ω is the angular frequency, and μ and σ are the permeability and conductivity of the conductor, respectively. The above distance $\delta_{\rm s}$ is the so-called skin depth.

The conductor loss of the solid CPW $\alpha_{\rm c}$ can be expressed as [24]

$$\alpha_{\rm c} = \frac{A}{\sigma\delta_{\rm s}}, \tag{2}$$

where A is a constant depending on the impedance and dimensions of the CPW. According to (1) and (2), the higher the frequency, the smaller the skin depth $\delta_{\rm s}$, and the higher the conductor loss $\alpha_{\rm c}$. For the laminated CPW, its conductor loss $\alpha_{\rm cL}$ can be expressed similarly to that of the solid CPW, which is

$$\alpha_{\rm cL} = \frac{A}{\sigma_{\rm e}\delta_{\rm se}}, \tag{3}$$

where $\sigma_{\rm e}$ and $\delta_{\rm se}$ are the effective conductivity and effective skin depth of the laminated conductor, respectively, which are expressed as [20]

$$\delta_{\rm se} = \sqrt{B}\left(1+\frac{t_1}{t_2}\right)\left(\frac{\delta_{\rm s}}{t_1}\right)\delta_{\rm s}, \tag{4}$$

$$\sigma_{\rm e} = \sigma\left(\frac{t_1}{t_1+t_2}\right), \tag{5}$$

where B is a constant depending on the structure of the interconnect.

According to [20], due to the introduction of the insulators, $\delta_{\rm se}$ is larger than $\delta_{\rm s}$ and $\sigma_{\rm e}$ is smaller than σ, when the frequency f is lower than a critical value $f_{\rm s}$, and the conductor loss is governed by $\delta_{\rm se}$ when $f \geqslant f_{\rm s}$, $\delta_{\rm se}$ is equal to $\delta_{\rm s}$ and $\sigma_{\rm e}$ is equal to σ. From (2) and (3), the conductor loss of the laminated CPW is smaller than that of the solid CPW when $f < f_{\rm s}$ and is similar to that of the solid CPW when $f \geqslant f_{\rm s}$. The critical frequency $f_{\rm s}$ is approximately expressed as [20]

$$f_{\rm s} = \frac{B}{\pi\mu_0\sigma {t_1}^2}, \tag{6}$$

where μ_0 is the permeability of the vacuum. In Figure 5, sketches of the conductor loss curves of the laminated CPW and solid CPW are drawn.

3.2 Simulation of the laminated CPW

As the critical frequency $f_{\rm s}$ is proportional to the square of t_1, the constant B for the proposed laminated CPW could be easily fitted through a full-wave simulation. As shown in Table 1, several groups of laminated CPWs with different sizes and different t_1 are listed, where all the CPWs are designed as 50 Ω. By comparing the conductor losses of the laminated CPWs and their corresponding solid CPWs, $f_{\rm s}$ of

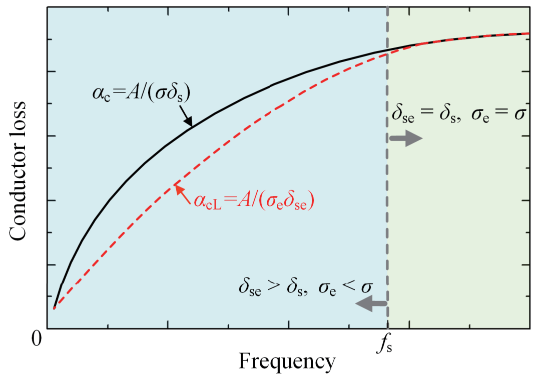

Figure 5 (Color online) Conductor losses of the laminated CPW and solid CPW.

Table 1 Size dimensions of the laminated CPWs for fitting B

Group	Dimensions (µm)	ϵ_2	Insulator layers (n)	t_1 (µm)	t_2 (µm)
1	$g = 10, w_s = 64$	4.7	1,2,3	$1.98/(n+1)$	$0.06/n$
2	$g = 10, w_s = 58$	4.7	3	0.66	0.02
3	$g = 10, w_s = 52$	4.7	4	0.66	0.02
4	$g = 10, w_s = 59$	4.7	1,2,3	$2.7/(n+1)$	$0.06/n$
5	$g = 15, w_s = 100$	4.7	1,2,3	$1.98/(n+1)$	$0.06/n$
6	$g = 10, w_s = 39$	6.2	1,2,3	$2.4/(n+1)$	$0.06/n$
7	$g = 10, w_s = 186$	2.2	1,2,3	$3/(n+1)$	$0.06/n$

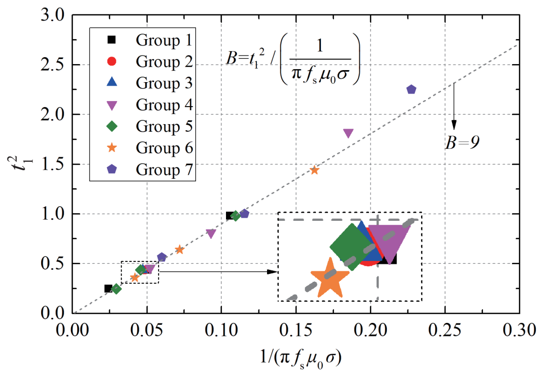

Figure 6 (Color online) Relationship between t_1 and f_s for fitting B.

each laminated CPW can be obtained. Then, the relation between t_1 and f_s is drawn in Figure 6, and the constant B could be fitted as 9. Thus, f_s and δ_{se} of the proposed laminated CPW are expressed as

$$\delta_{se} = 3\left(1+\frac{t_1}{t_2}\right)\left(\frac{\delta_s}{t_1}\right)\delta_s, \tag{7}$$

$$f_s = \frac{9}{\pi\mu_0\sigma {t_1}^2}. \tag{8}$$

The effective skin depth δ_{se} depends on t_1, t_2, and δ_s. To obtain a laminated CPW with a lower conductor loss than that of the solid CPW over the millimeter-wave frequency band, that is, f_s larger than 30 GHz, the single metal thickness of the laminated conductor t_1 should be smaller than 1.1 µm for the laminated conductor with silver according to (8).

3.3 Effects of the laminated conductor on the CPW

To illustrate the effect of the laminated conductor on the propagation properties of the laminated CPW, four laminated CPWs and a solid CPW are analyzed based on a full-wave simulation. Table 2 lists the size dimensions of the five CPWs. The designs of the laminated CPWs I, II, and III are from Group 1

Table 2 Size dimensions of the laminated CPWs for the property analysis

Structure	Insulator layers (n)	t_1 (μm)	t_2 (μm)	f_s
Soldi CPW	0	2.04	0	–
Laminated CPW I	1	0.99	0.06	44
Laminated CPW II	2	0.66	0.03	86
Laminated CPW II*	2	0.66	0.03	86
Laminated CPW III	3	0.495	0.02	162

in Table 1. The dimensions of the laminated CPW II* are absolutely the same as those of the laminated CPW II, but the laminated CPW II* is only equipped with a laminated conductor as its signal line and a solid conductor as its ground line, whereas the laminated CPW II is equipped with a laminated conductor as its ground and signal line. The signal width w_s and gap width g of the CPWs are determined as 64 and 10 μm, respectively. The thickness of the silica glass wafer h is 1 mm. The CPWs are designed with the same conductor thickness t, which is 2.04 μm. The laminated CPWs with different insulator layers have different conductor thickness t_1 and insulator thickness t_2, but the total thickness of the conductor and insulator keep to constants, which are 60 and 1980 μm, respectively.

Based on the Ansys high-frequency structure simulator, the propagation properties of the five CPWs are simulated and plotted in Figures 7 and 8. The characteristic impedance of the five CPWs is simulated and drawn in Figure 7(a), where the characteristic impedance of all the CPWs is 50 Ω. The simulated phase constants of the CPWs show the same linear relationship versus frequency in Figure 7(b). The simulated attenuation constants versus the frequency of the CPWs are illustrated in Figure 7(c), where the dielectric attenuation of the CPWs is the same. Therefore, replacing the solid conductor with the laminated conductor has nearly no impact on the characteristic impedance, phase constant, and dielectric attenuation. This makes sense because CPWs have exactly the same substrate and conductor sizes. As shown in Figure 7(c), the conductor attenuation of the laminated CPWs is larger than that of the solid CPW. For example, the conductor attenuation of the solid CPW is 30 times its conductor attenuation at 40 GHz. The super-narrow line/gap width of the CPWs causes a sharp increase in the conductor attenuation, and hence it dominates the total attenuation constant. The conductor attenuation of all the laminated CPWs is less than that of the solid CPW. For instance, the conductor attenuations of the laminated CPW II and solid CPW are 0.11 and 0.14 dB/mm at 40 GHz, respectively. The laminated CPW with many insulator layers shows a low conductor attenuation and high linear relation between the conductor attenuation and frequency. The conductor attenuation curves of the laminated CPWs I and II overlap with that of the solid CPW at 44 and 86 GHz, respectively, which agrees with the calculated fs from (5). Compared with the solid CPW, the conductor attenuation reduction of the laminated CPW II* is around half that of the laminated CPW II. Hence, applying the laminated conductor to the ground is as effective as applying it to the signal line for the proposed laminated CPW. Moreover, the simulated S-parameters of the five CPWs with transitions ($l_1 = 9$ mm, $l_2 = l_3 = 0.1$ mm) are plotted in Figure 8. The S21 parameters of the CPWs in Figure 8(a) show an attenuation consistent with that in Figure 7(c) and the attenuation of the laminated CPWs is smaller than that of the solid CPW. The S11 parameters of different CPWs are nearly the same, which are smaller than −18 dB from DC to 100 GHz.

4 Fabrication and experiment

4.1 Fabrication and measurement setup

To verify the low-loss property of the proposed laminated CPW, a laminated CPW II and solid CPW are fabricated with the developed processes, and their S-parameters are measured. The length of the CPWs l_1 is 9 mm, and the overlapping part length l_2 and connecting part length l_3 of the transition are set as 0.1 mm. The measurement environment is shown in Figure 9(a), where the CPWs are connected to a vector network analyzer (VNA) by two ground-signal-ground (G-S-G) probes. A photo of the fabricated laminated CPW and solid CPW is shown in Figure 9(b). Limited by our VNA and probes, the measurement is carried out from DC to 40 GHz.

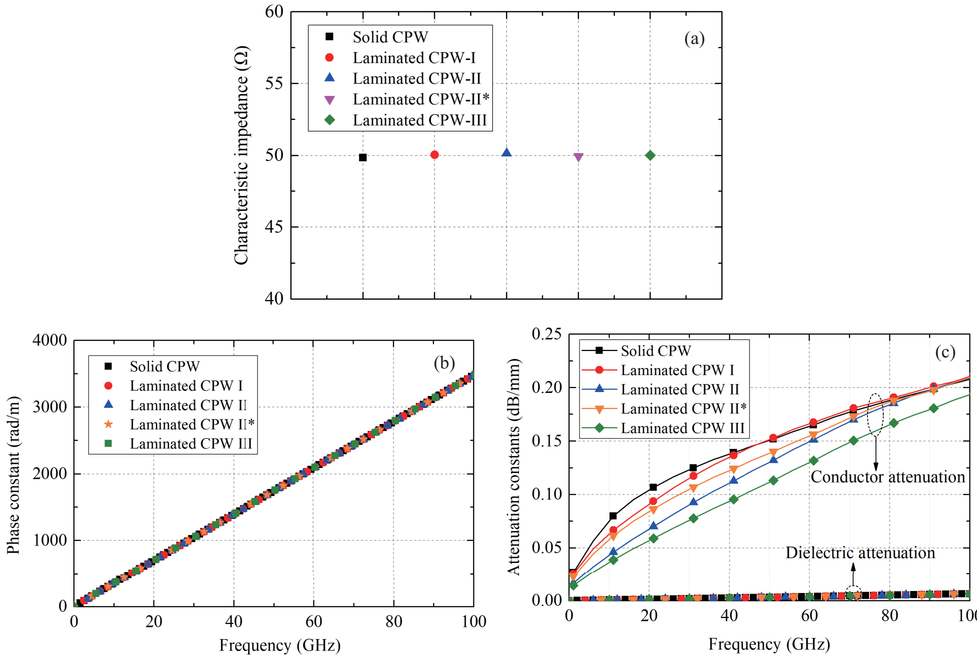

Figure 7 (Color online) (a) Characteristic impedance of the CPWs; (b) phase constants of the CPWs versus frequency; (c) attenuation constants of the CPWs versus frequency.

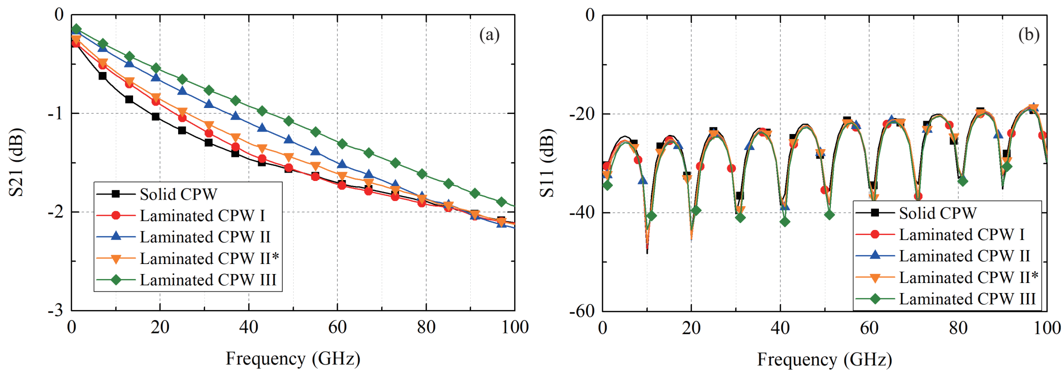

Figure 8 (Color online) S-parameters of the CPWs. (a) S21 parameters; (b) S11 parameters.

4.2 Measurement results

The measured and simulated S-parameters of the laminated CPW and solid CPW are drawn in Figure 10. In Figure 10(a), the simulated S11 of the two CPWs are nearly the same and smaller than −22 dB, and the measured S11 of the laminated CPW is a little larger than that of the solid CPW over 25 GHz and are smaller than −13 dB from DC to 40 GHz. The fabrication process of the laminated CPW is more complicated than that of the solid CPW and the manufacturing error of the laminated CPW introduces a larger impedance mismatching than that of the solid CPW. As shown in Figure 10(b), the simulated and measured S21 parameters of the laminated CPW are larger than those of the solid CPW. From DC to 40 GHz, the average measured S21 of the laminated CPW and solid CPW are −0.65 and −1.17 dB, respectively. The average insertion loss of the laminated CPW is 44.4% smaller than that of the solid CPW from DC to 40 GHz. The low insertion loss of the laminated CPW is attributed to the low conductor loss of the laminated CPW, which is proven in Figure 7(c).

4.3 Performance comparison with the state of the arts

The performances of the proposed laminated CPW and the state of the art are compared in Table 3. The suspended strip line [15] with a symmetrical metal worked from 8 to 11 GHz, whose loss was 30% smaller than that of the conventional suspended strip line at 10 GHz. CPWs [17,19] using magnetic-multilayered

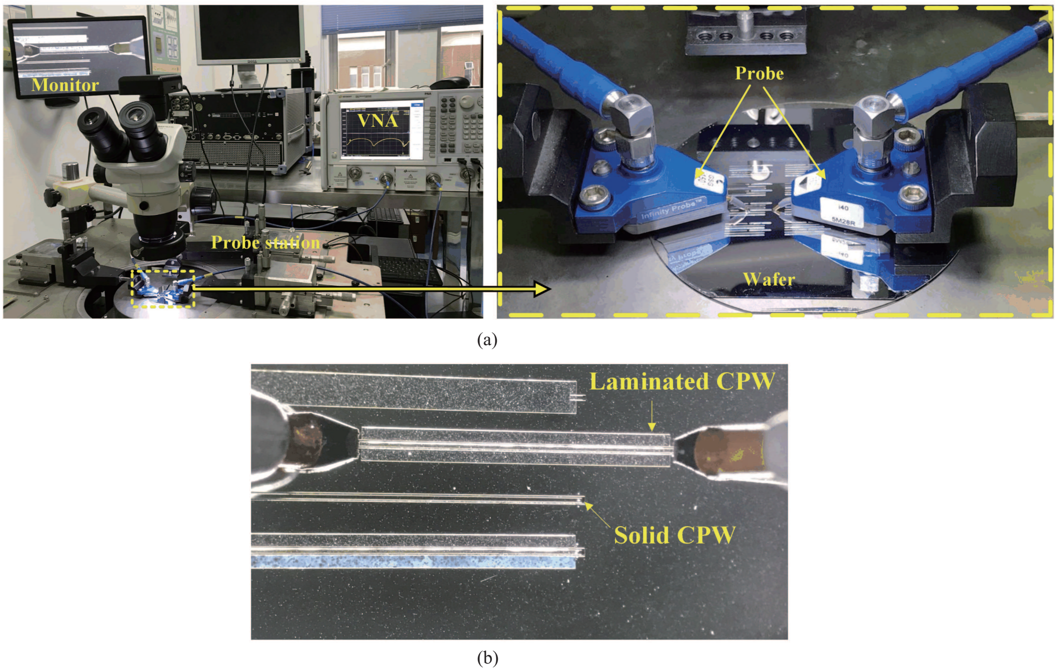

Figure 9 (Color online) Photos of the measurement setup. (a) Measurement environment of the probe stations; (b) fabricated laminated CPW and solid CPW.

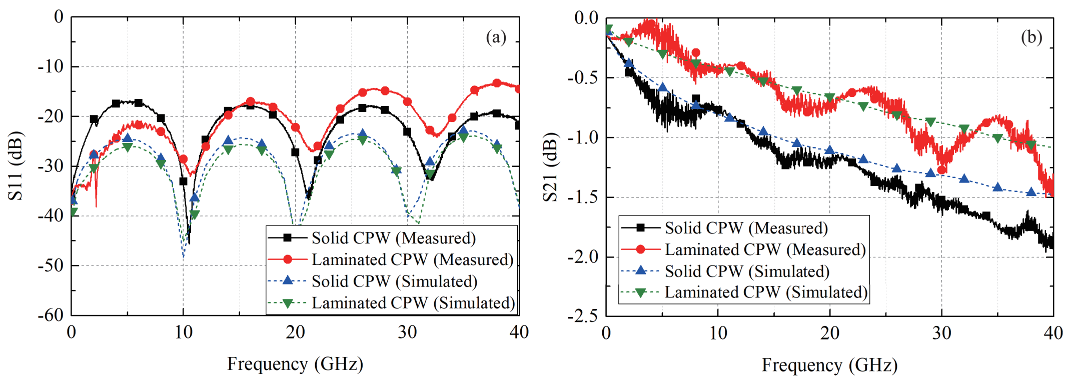

Figure 10 (Color online) S-parameters of the laminated CPW and solid CPW. (a) S11 parameters; (b) S21 parameters.

Table 3 Comparison between the laminated CPW and the state of the art

Structure	Method	Layers of metal	Line width (mm)	Bandwidth (GHz)	Loss reduction	Technology	Planar integrated
Suspended stripline [15]	Symmetrically-metal	2	0.5	8–11	30% @ 10 GHz	PCB	YES
CPW [17]	Magnetic-multilayered	16	0.09	0–15	50% @ 14 GHz	Silicon-based MEMS	YES
CPW [19]	Magnetic-multilayered	10	0.1	0–32	50% @ 28 GHz	Silicon-based MEMS	YES
Coaxial line [21]	Laminated conductor	100	–	0–0.025	40% @ 12 MHz	Mechanical	NO
CPW (this work)	Laminated conductor	3	0.064	0–40	55% @ 35 GHz Average 44.4%	Silicon-based MEMS	YES

technology worked from DC to 15 GHz and DC to 32 GHz, and their losses reduction can be up to 50% compared with solid CPWs. However, their magnetic materials resulted in concerns about the EMC problem. The laminated coaxial line [21] only worked from DC to 25 MHz with up to 40% loss reduction, where its laminated conductor consists of 100 layers of metal. The proposed laminated CPW has the widest operation bandwidth from DC to 40 GHz, which shows a 55% loss reduction than the solid CPW at 35 GHz and a 44% average loss reduction from DC to 40 GHz. Moreover, the laminated CPW has only three layers of stacked metal, much smaller than the CPWs [17, 19].

5 Conclusion

In this paper, the laminated conductor is first introduced to the planar integrated transmission line and applied for wide-bandwidth low-loss millimeter-wave transmission. In the case of the CPW, a laminated CPW is proposed. Based on the silicon-based MEMES technology, the laminated CPW with its transitions is designed, fabricated, and measured. Simulation results illustrate that replacing the solid conductor of the CPW with the laminated conductor shows lower conductor loss and has nearly no impact on the characteristic impedance, phase constant, and dielectric attenuation of the CPW. Measurement results show that the insertion loss of the laminated CPW is obviously less than that of the solid CPW from DC to 40 GHz, where the average insertion loss reduction is 44.4%. In summary, the proposed laminated CPW shows significantly lower loss than the conventional solid CPW, which is suitable for low-loss and high-density millimeter-wave interconnect.

Acknowledgements This work was supported by National Natural Science Foundation of China (Grant No. 61831016) and Guangdong Provincial Key-Field Research Program (Grant No. 2018B010115001).

References

1 Tam S W, Chang M C F. RF/wireless-interconnect: the next wave of connectivity. Sci China Inf Sci, 2011, 54: 1026–1038
2 Hao Y, Xiang S, Han G, et al. Recent progress of integrated circuits and optoelectronic chips. Sci China Inf Sci, 2021, 64: 201401
3 Casimir H, Ubbink J. The skin effect. I. introduction the current distribution for various configurations. Philips Tech Rev, 1967, 28: 271–283
4 Tolpygo S, Bolkhovsky V, Weir T, et al. Advanced fabrication processes for superconducting very large scale integrated circuits. IEEE Trans Appl Supercond, 2016, 26: 1100110
5 U-Yen K, Rostem K, Wollack E J. Modeling strategies for superconducting microstrip transmission line structures. IEEE Trans Appl Supercond, 2018, 28: 1–5
6 Ji L Y, Ma J, Sun J, et al. Design and performance of dual-band high temperature superconducting filter. Sci China Inf Sci, 2012, 55: 956–961
7 Li Y, Li X C, Yang Y, et al. An unconditionally stable 2-D stochastic WLP-FDTD method for geometric uncertainty in superconducting transmission lines. IEEE Trans Appl Supercond, 2022, 32: 1–9
8 Yang Y, Li X C, Li Y, et al. A compact 2-D stochastic FDTD method for uncertainty analysis in superconducting transmission lines. IEEE Trans Appl Supercond, 2020, 30: 1–7
9 Pei Z W, Li X C, Li Y, et al. Transient coanalysis of multicoupled passive transmission lines and josephson junctions based on FDTD. IEEE Trans Appl Supercond, 2020, 30: 1–7
10 Wu R, Zhu R Z, Zhao S H, et al. Filling the gap: thermal properties and device applications of graphene. Sci China Inf Sci, 2021, 64: 140401
11 Zhao D, Fan F, Li T, et al. Terahertz magneto-optical isolator based on graphene-silicon waveguide. Sci China Inf Sci, 2022, 65: 169401
12 Sarafis P, Hsu C L, Benech P, et al. Cu nanolines for RF interconnects: electrical characterization. IEEE Trans Electron Dev, 2015, 62: 1537–1543
13 Wallis T, Kim K, Filipovic D, et al. Nanofibers for RF and beyond. IEEE Microw, 2011, 12: 51–61
14 Kuroki F, Tamaru R, Masumoto R, et al. Loss reduction technique of printed transmission line at millimeter-wave frequency. In: Proceedings of IEEE/MTT-S International Microwave Symposium, Honolulu, 2007. 1671–1674
15 Cui L, Wu W, Fang D G. Low loss slow-wave unit based on even-mode bilateral broadside-coupled suspended microstrip line. In: Proceedings of Cross Strait Quad-Regional Radio Science and Wireless Technology Conference, Harbin, 2011. 463–467
16 Rejaei B, Vroubel M. Suppression of skin effect in metal/ferromagnet superlattice conductors. J Appl Phys, 2004, 96: 6863–6868
17 Zhuang Y, Rejaei B, Schellevis H, et al. Magnetic-multilayered interconnects featuring skin effect suppression. IEEE Electron Device Lett, 2008, 29: 319–321
18 Sato N, Endo Y, Yamaguchi M. Skin effect suppression for Cu/CoZrNb multilayered inductor. J Appl Phys, 2012, 111: 07A501
19 Hwangbo S, Rahimi A, Yoon Y K. Cu/Co multilayer-based high signal integrity and low RF loss conductors for 5G/millimeter wave applications. IEEE Trans Microw Theor Techn, 2018, 66: 3773–3780
20 Clogston A. Reduction of skin-effect losses by the use of laminated conductors. Proc IRE, 1951, 39: 767–782
21 King R A. An experimental clogston 2 transmission line. Bell Syst Technical J, 1959, 38: 517–536
22 Black H, Mallinckrodt C, Morgan S. Experimental verification of the theory of laminated conductors. Proc IRE, 1952, 40: 902–905
23 Pozar D. Electromagnetic theory. In: Microwave Engineering. 4th ed. New York: Wiley, 2012. 95–164
24 Grag R. Coplanar lines. In: Microstrip Lines and Slot Lines. 3th ed. Boston: Artech House, 2013. 387–392